Journal of Power Sources 196 (2011) 9018–9021

Contents lists available at ScienceDirect

Journal of Power Sources

journal homepage: www.elsevier.com/locate/jpowsour

Short communication

Stress analysis of solid oxide fuel cell anode microstructure reconstructed from focused ion beam tomography

R. Clague[a,*], P.R. Shearing[b], P.D. Lee[d], Z. Zhang[d], D.J.L. Brett[c], A.J. Marquis[e], N.P. Brandon[a]

[a] Energy Futures Lab, Imperial College London, South Kensington, SW7 2AZ, UK
[b] Department of Earth Science and Engineering, Imperial College London, London, UK
[c] Department of Chemical Engineering, UCL, London, UK
[d] Department of Materials, Imperial College London, London, UK
[e] Department of Mechanical Engineering, Imperial College London, London, UK

ARTICLE INFO

Article history:
Received 31 October 2010
Received in revised form
20 December 2010
Accepted 22 December 2010
Available online 13 January 2011

Keywords:
SOFC
Tomography
Stress analysis

ABSTRACT

The degradation and ultimately lifetime of solid oxide fuel cells (SOFCs) is determined in part by the stresses generated within the different layers of the device. For fully dense materials such as the electrolyte, when modelling these stresses on a macro-scale the material properties can be considered to be homogeneous (evenly distributed) allowing the prediction of volume average stresses due to differential thermal expansion in the layer. However, detailed stress analysis of real, multiphase porous layers such as those found in SOFC electrodes, on the micron and sub-micron scale has not been possible to date as detailed geometry and convenient methods to generate a finite element model have not been available.

In this paper we present work that combines microstructural characterisation of a porous solid oxide fuel cell anode with three dimensional stress analysis to inspect the stresses within the individual phases of the anode, and at phase boundaries. The electrode microstructure has been characterised using focused ion beam (FIB) tomography and the resulting microstructure used to generate a solid mesh of three dimensional tetrahedral elements. A temperature field was applied to simulate the heating of the sample from room temperature (298 K) to operating temperature (1073 K). The maximum principal stress in the nickel phase was found to exceed the yield strength, while the minimum principal stress in the yttria-stabilized zirconia (YSZ) phase was found to exceed the characteristic strength of that volume of YSZ, indicating that the probability of failure of the YSZ matrix is significant.

1. Introduction

Solid oxide fuel cells (SOFCs) are a high temperature fuel cell variant that employ oxide ion conducting ceramic electrolytes operating in the temperature range of 500–1000 °C. These devices show excellent potential for a broad range of power generation applications and particularly for large scale and residential combined heat and power (CHP) [1]. However, elevated temperature operation imparts certain challenges, not least the management of mechanical stresses due to differential thermal expansion between layers, and between different phases within the electrode layers.

The Ni-YSZ (yttria-stabilized zirconia) cermet is a common choice for the anode material of SOFCs in both electrolyte supported and anode supported geometries owing to its low-cost, thermal and chemical stability, good electronic conductivity, and high catalytic activity for hydrogen oxidation [2]. Providing intimate contact of ionic, electronic and pore phases at triple phase boundaries (TPBs) is critical to optimising electrochemical performance. In these composite porous anodes, TPBs are distributed throughout the electrode bulk.

Recently, the use of advanced focused ion beam (FIB) and X-ray nanofocus computed tomography (nano-CT) techniques has enabled direct access to information on the spatial distribution of TPBs in an SOFC electrode structure (e.g. [3–10]). These tomographs provide unprecedented detail regarding the complex microstructure of SOFC electrodes and can be used to understand evolution and degradation mechanisms during processing and operation. However, these tomographic techniques are perhaps most powerful when utilised in tandem with numerical simulation to explicitly evaluate the influence of microstructural heterogeneities, as demonstrated previously in other materials ranging from metal matrix composites [11] to glass foams [12].

The literature provides a wealth of electrode modelling studies exploring processing, electrochemical operation and mechanical performance. These models typically adopt some microstructural framework of varying complexity in two or three dimensions; indeed there has been significant effort in developing tools for generation of microstructural analogues [13–15]. While these tools

* Corresponding author. Tel.: +44 0 20 7594 1539; fax: +44 0 20 7594 6566.
E-mail address: r.clague@imperial.ac.uk (R. Clague).

0378-7753/$ – see front matter © 2011 Elsevier B.V. All rights reserved.
doi:10.1016/j.jpowsour.2010.12.097

are increasingly capable of generating realistic microstructural analogues they remain idealised representations. The ability to interface tomographic techniques with relevant simulations is therefore highly desirable.

A number of groups have recently demonstrated this capability: Shearing et al. utilised a volume of fluid (VOF) model to predict electrochemical performance in a Ni-YSZ anode [16]. Using voxelised FIB data, the microstructure was discretised into ca. 8000 elements, transport phenomena and electrochemical behaviour was modelled in each of the VOF elements providing a prediction of the spatial distribution of current generation.

Lattice Boltzmann methods have also been successfully applied to SOFC reconstructions from FIB tomography [4] and X-ray nano-CT [7,9]. These methods enable the direct use of voxelised data without the requirement for "coarse-meshing". However, the techniques are computationally expensive, often requiring access to high performance super computers to model representative volume elements. Recently Chiu et al. estimated that using a linearly scaled Lattice Boltzmann model for methane reforming in a real-life microstructure obtained from tomography experiments would take up to 8 weeks on a 2000 processor facility [17].

Wilson et al. demonstrated the potential for combining FE models with tomography data for prediction of gas phase tortuosity [3]. However, the community has typically been constrained by the ability to generate high quality meshes for conventional FE analysis – in the authors' experience meshing tools can be liable to artefacts (particularly at interfaces) which require laborious manual repair. The ability to accurately mesh microstructural tomography data for combination with FE simulations will provide a powerful tool.

Here we present the combination of FIB tomography data with mechanical stress simulation. A tetrahedral finite element mesh was successfully created from the reconstructed tomography surfaces using commercially available software (Scan FE, Simpleware Ltd., Exeter).

2. Microstructure reconstruction

2.1. FIB technique

Electrolyte supported Ni-YSZ symmetrical cells were manufactured by screen printing commercially available NiO-YSZ ink (Ceramtec, Germany) onto commercially available tape-cast electrolyte supports (Nextec Inc. USA). The half cells were subsequently chemically reduced and characterised using electrochemical impedance spectroscopy (see [16]) Following electrochemical testing, FIB tomography was used to characterise the Ni-YSZ electrode microstructure using a Zeiss xB-1540 FIB-FEG SEM at the London Centre for Nanotechnology.

Using the dual beam FIB to sequentially mill and image the Ni-YSZ electrode structure, a sequence of 170 images was collected; pixel dimensions of 20 nm were recorded with an inter-slice thickness of 15 nm. From this sequence, 100 images were selected and segmented for further analysis. Further details of the tomography data collection have been published elsewhere [16].

The total reconstructed volume is $6.68 \times 5.04 \times 1.50\ \mu m$. While larger reconstructions have been conducted (e.g. [5,8]) this volume is representative of the screen-printed electrode, which has a thickness of 5 μm. The total TPB density measured following a technique described by Shearing et al. [16] is $12.99\ \mu m^{-2}$ with volume fractions Ni = 35.5%, YSZ = 46.7% and pore = 17.8%.

3. Finite element model

The finite element (FE) model was generated from the segmented tomography data using ScanFE software (ScanFE V3.1, Simpleware Ltd, UK). The FE model consisted of 285,000 four-node tetrahedral elements (Abaqus type C3D4). The appropriate number of elements was determined from a mesh independence test, which showed that mesh independent stress results based on average stress were obtained at this element density. During meshing the Ni and YSZ phases were assigned to one of two material sections to allow allocation of appropriate material properties, as shown in Fig. 1(a) and (b). Node and element sets were automatically generated on the model cut planes and at the interface of the two phases.

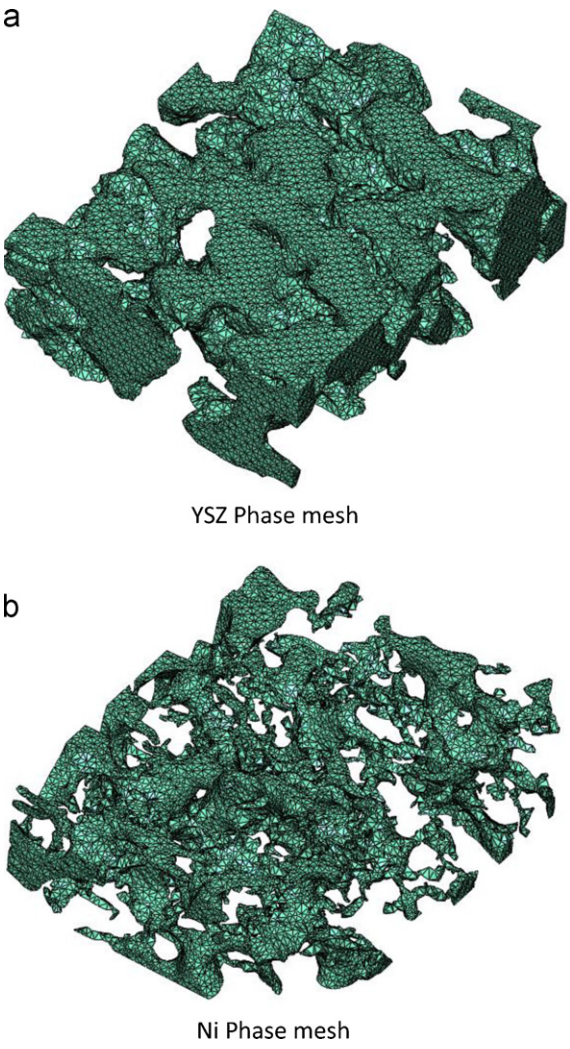

Fig. 1. (a) YSZ phase mesh, (b) Ni phase mesh

Boundary conditions and load-cases in the form of a global temperature field were applied (as detailed below) using Abaqus CAE (v6.10, Simulia, UK) and finally a stress analysis was run using the Abaqus Implicit finite element solver. The analysis assumed that there was no separation of the Ni and YSZ phases and that the material behaviour was linear and elastic.

The simulation took 89 s to complete on a computer with a Linux operating system using four AMD Opteron dual core 64 bit processors and a 2 GHz clock speed.

3.1. Boundary conditions

In order to represent the reconstructed portion of the electrode as a section of a larger anode, the boundary conditions that were applied to the model constrained the cut planes to remain pla-

Table 1
Material properties.

Layer	Material	Temperature (K)	E	ν	α ($\times 10^{-6}$)	Yield (MPa)	UTS (MPa)
Anode	Ni [18]	1073	207	0.31	13.5	59	317
	YSZ [19]	1073	157	0.313	10.5	n/a	n/a

nar, while allowing bulk thermal expansion between opposite cut planes. This was achieved by restraining the degree of freedom of the nodes on one cut plane in the direction normal to the cut plane, then on the opposite cut plane the normal degree of freedom of the nodes on that plane were tied together. This has the effect of allowing bulk thermal expansion between opposing cut planes, while still imposing the condition that the cut planes remain planar. These mechanical boundary conditions are not considered to fully represent the behaviour of the cut planes of the sample were it in a fuel cell, but this will be investigated in due course through sub-modelling.

As the YSZ phase is wetted by the Ni phase, a strain continuity condition was imposed at the interface between the Ni and YSZ phases. The solid phases were free to expand into the pore phase. A global temperature field T_0 of 298 K was applied as an initial, zero stress condition, which was subsequently increased to a temperature T_1 of 1073 K in a single analysis step.

3.2. Material properties

The mechanical properties of the materials required for the thermo-mechanical stress analysis are summarised in Table 1. E is the elastic modulus (GPa) ν is the dimensionless Poisson's ratio and α is the coefficient of thermal expansion ($1\,K^{-1}$).

4. Results

4.1. Stress analysis

The differential thermal expansion of the Ni and YSZ phases generates stresses within the composite structure that peak at the interfaces of the solid phases. Figs. 2(a), (b) and 3 shows the maximum principal stress field generated when the global temperature of the composite structure changes from T_0 to T_1. In the Ni phase the peak maximum principal stress of over 200 MPa is a significant proportion of the failure strength of 317 MPa, and well above the yield strength of 57 MPa at 1073 K, illustrating that the elastic analysis used is a simplifying approximation that will over-estimate peak stresses.

5. Discussion

The stresses predicted by this analysis exceed the yield strength of the Ni phase by some margin, implying that stress relief through plastic deformation is likely to occur at the phase boundaries as the sample is heated from room to operating temperature. By assuming perfectly elastic material behaviour and a zero stress state at room temperature, the analysis predicts that plastic deformation would occur within the Ni phase near the phase boundary. Unfortunately the strength of the Ni-YSZ interface is not known so no comment can be made on whether delamination is expected.

In the YSZ phase the minimum principal stress has a magnitude of over 200 MPa. The failure strength of YSZ is not a simple matter to determine as it is a brittle material and therefore the failure strength is volume dependent [20]. It is more usual to consider probability of failure when talking about brittle materials but in this analysis, in order to qualitatively examine whether the stresses are more likely than not to cause failure the stresses are simplistically compared to the characteristic strength, σ_θ, of the YSZ phase,

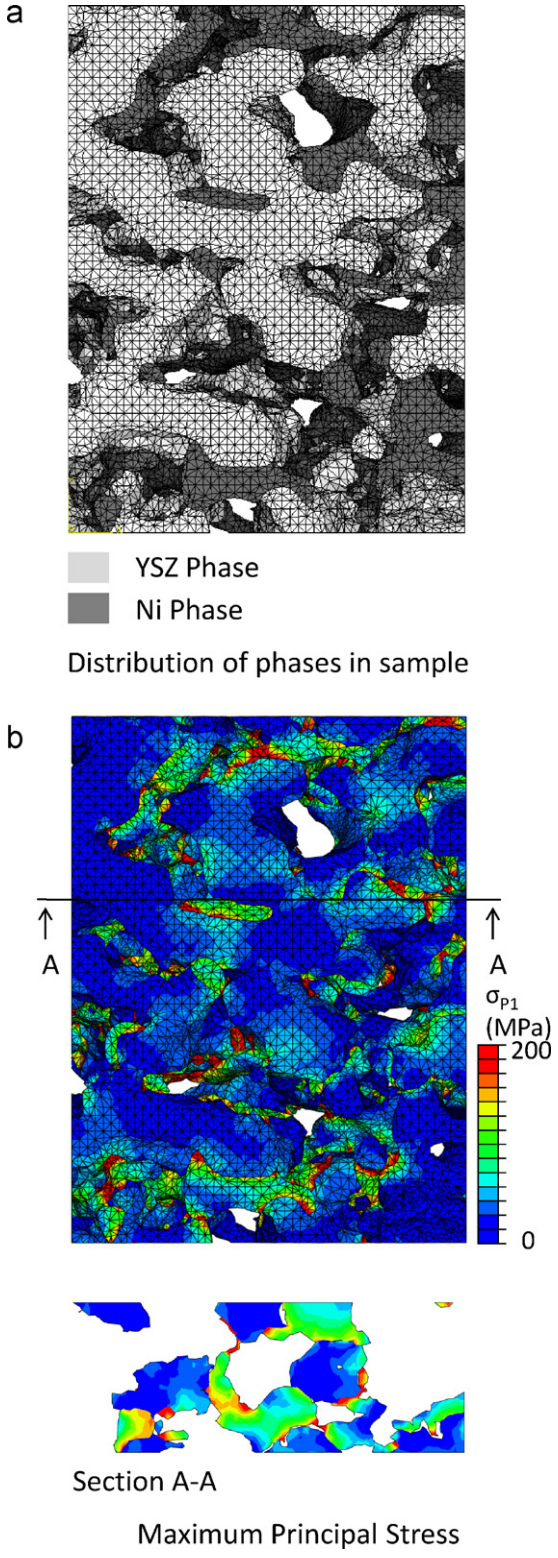

Fig. 2. (a) Distribution of phases, (b) maximum principal stress

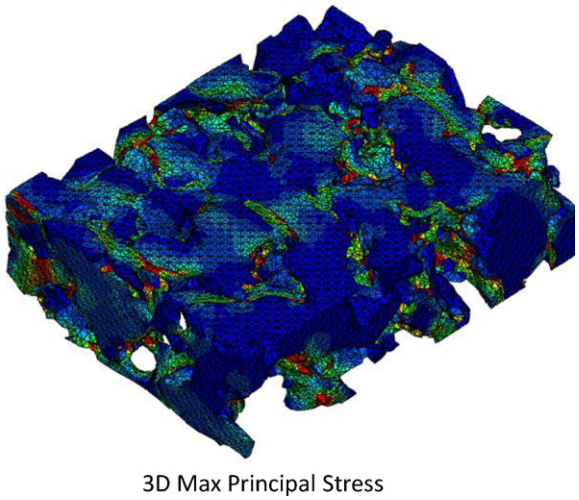

Fig. 3. 3D max principal stress

defined as the stress at which 50% of samples of this structure would fail. For the purposes of this analysis the volume of material, V_e was taken to be equal to the volume of the reconstructed sample and σ_θ was calculated from Equation (1). The material property σ_0, is defined as the stress at which samples of the material of unit volume would fail. The values used here are taken as $\sigma_0 = 23.1$ MPa [21], the Weibull modulus $m = 8.6$ [19], and $V_e = 50 \times 10^{-9}$ m^3, giving a value of $\sigma_\theta = 163$ MPa.

$$\sigma_\theta = \sigma_0 (V_e)^{-\frac{1}{m}} \quad (1)$$

Assuming the failure characteristics of YSZ are the same in compression and tension, the characteristic strength of YSZ at these volumes is therefore exceeded, so from the results of this analysis some fracturing of the ceramic matrix would be expected. In this analysis linear elastic material properties have been assumed, which will tend to over predict stress levels, as plastic deformation in the nickel phase will tend to relieve stress. A time dependent elastic–plastic analysis of the structure is expected to predict lower final stress levels and therefore a lower probability of failure. While a calculation of the probability of failure of the structure is beyond the scope of this paper, using a method demonstrated by Clague [21] the probability of failure of each finite element of the ceramic phase can be calculated, as the mean stress and volume of each finite element are known. The probability of failure for the entire phase can then be calculated by summing the individual failure probabilities of the finite elements following the Weibull weakest link theory [20].

6. Conclusion

This work has demonstrated the viability of a technique to capture real, highly complex, two phase microstructural geometry such as that found in SOFC electrodes using FIB tomography and generate a finite element model of suitable quality for thermo-mechanical stress analysis from it. Using simple elastic analysis, the method was shown to be a potentially powerful tool for studying the response of complex multiphase structures to thermally, mechanically or chemically induced stress. The key result in this work is that the yield strength of nickel is exceeded at the interface of the Ni and YSZ phases, indicating that this is potentially an important mechanism for stress relief in SOFC electrodes as they are heated or cooled.

The authors are presently developing a technique to examine the normal stresses at phase boundaries, allowing a prediction of TPB movement or loss when compared to the work of adhesion of Ni on YSZ. This technique offers the possibility of studying the stresses within, and failure mechanisms of, the nickel and YSZ phases. This method also has application as a submodelling technique, with displacement boundary conditions applied at the model cut planes from a macro-scale stress analysis.

Acknowledgments

The authors acknowledge the financial support of the EPSRC Supergen Fuel Cells programme. Focused ion beam work was carried out at the ion beam facility at the London Centre for Nanotechnology.

References

[1] A.D. Hawkes, I. Staffell, D.J.L. Brett, N.P. Brandon, Energy & Environmental Science 2 (7) (2009) 729–744.
[2] Z. Cheng, J. Wang, M. Liu, in: J.W. Fergus, et al. (Eds.), Solid Oxide Fuel Cells—Materials Properties and Performance, CRC Press, Boca Raton, 2009.
[3] J.R. Wilson, W. Kobsiriphat, R. Mendoza, H.Y. Chen, J.M. Hiller, D.J. Miller, K. Thornton, P.W. Voorhees, S.B. Adler, S.A. Barnett, Nature Materials 5 (7) (2006) 541–544.
[4] N. Shikazono, D. Kanno, K. Matsuzaki, H. Teshima, S. Sumino, N. Kasagi, Journal of the Electrochemical Society 157 (5) (2010) B665–B672.
[5] P.R. Shearing, J. Golbert, R.J. Chater, N.P. Brandon, Chemical Engineering Science 64 (17) (2009) 3928–3933.
[6] P.R. Shearing, J. Gelb, J. Yi, W.K. Lee, M. Drakopolous, N.P. Brandon, Electrochemistry Communications 12 (8) (2010) 1021–1024.
[7] J.R. Izzo, A.S. Joshi, K.N. Grew, W.K.S. Chiu, A. Tkachuk, S.H. Wang, W.B. Yun, Journal of the Electrochemical Society 155 (5) (2008) B504–B508.
[8] H. Iwai, N. Shikazono, A. Matsui, H. Teshima, M. Kishimoto, R. Kishida., K. Matsuzaki, D. Kanno, M. Saito, H. Muroyama, K. Eguchi, N. Kasagi, H. Yoshida, Journal of Power Sources 195 (4) (2009) 955–961.
[9] K.N. Grew, Y.S. Chu, J. Yi, A.A. Peracchio, J.R. Izzao, Y. Hwu, F. De Carlo, W.K.S. Chiu, Journal of the Electrochemical Society 157 (6) (2010) B783–B792.
[10] P.R. Shearing, D.J.L. Brett, N.P. Brandon, International Materials Reviews 55 (6) (2010) 347–363.
[11] I.G. Watson, P. Lee, R. Dashwood, P. Young, Metallurgical Transactions A 37 (2006) 8–551.
[12] S.A. Sanchez, J. Narciso, F. Rodriguez-Reinoso, D. Bernard, I.G. Watson, P.D. Lee, R.J. Dashwood, Advanced Engineering Materials 8 (6) (2006) 491–495.
[13] J.I. Golbert, C.S. Adjiman, N.P. Brandon, Industrial Engineering Chemical Research 47 (20) (2008) 7693–7699.
[14] B. Kenney, M. Valdmani, C. Baker, J.G. Pharoah, K. Karan, Journal of Power Sources 189 (2) (2009) 1051–1059.
[15] S. Sunde, Journal of Electroceramics 5 (2) (2000) 153–182.
[16] P.R. Shearing, Q. Cai, J.I. Golbert, V. Yufit, C.S. Adjiman, N.P. Brandon, Journal of Power Sources 195 (15) (2010) 4804–4810.
[17] K.N. Grew, A. Joshi, W. Chiu, Fuel Cells 10 (6) (2010) 1143–1156.
[18] http://www.matweb.com/search/DataSheet.aspx?MatGUID=e6eb83327e534850a062dbca3bc758dc&ckck=1. 2010 [cited 2010 6th September].
[19] A. Atkinson, T.M.G.M. Ramos, Solid State Ionics 129 (1–4) (2000) 259–269.
[20] W. Weibull, Ingeniors Vetenskaps Akademien - Handlingar 151 (45) (1939).
[21] R. Clague, The Probability of Failure of Solid Oxide Fuel Cells by the Integrated Modelling of Multiple Physical Processes in Mechanical Engineering, Imperial College, London, 2008.